CONDENSED MATTER PHYSICS

Current-driven magnetization switching in ferromagnetic bulk Rashba semiconductor (Ge,Mn)Te

R. Yoshimi[1]*, K. Yasuda[2], A. Tsukazaki[3], K. S. Takahashi[1,4], M. Kawasaki[1,2], Y. Tokura[1,2]

Multiferroic materials with both ferroelectric and ferromagnetic orders provide a promising arena for the electrical manipulation of magnetization through the mutual correlation between those ferroic orders. Such a concept of multiferroics may expand to semiconductor with both broken symmetries of spatial inversion and time reversal, that is, polar ferromagnetic semiconductors. Here, we report the observation of current-driven magnetization switching in one such example, (Ge,Mn)Te thin films. The ferromagnetism caused by Mn doping opens an exchange gap in original massless Dirac band of the polar semiconductor GeTe with Rashba-type spin-split bands. The anomalous Hall conductivity is enhanced with increasing hole carrier density, indicating that the contribution of the Berry phase is maximized as the Fermi level approaches the exchange gap. By means of pulse-current injection, the electrical switching of the magnetization is observed in the (Ge,Mn)Te thin films as thick as 200 nm, pointing to the Rashba-Edelstein effect of bulk origin. The efficiency of this effect strongly depends on the Fermi-level position owing to the efficient spin accumulation at around the gap. The magnetic bulk Rashba system will be a promising platform for exploring the functional correlations among electric polarization, magnetization, and current.

INTRODUCTION

In semiconductors without inversion symmetry, spin-orbit interaction causes the spin splitting of the electronic band structure, as exemplified by Rashba (*1*, *2*) and Dresselhaus (*3*) effects. By applying electric field to those spin-polarized bands, the nonequilibrium spin accumulation occurs, that is, Edelstein effect (*4*). After the initial observations of the Edelstein effect in inversion broken semiconductors with Rashba and Dresselhaus components (*5*, *6*), the highly efficient spin-charge conversion by the Edelstein effect has been demonstrated for two-dimensional (2D) electronic systems such as interfaces with metal (*7*) or oxide (*8*) and surface states of topological insulators (*9*–*15*). Recently, the research field has expanded to 3D materials with bulk ferroelectric polarity. The characteristic materials endowed with the bulk Rashba effect are polar semiconductors, such as BiTe*X* (*X* = Cl, Br, I) (*16*, *17*) and GeTe (*18*–*20*). Among them, the magnetic ion (Mn) doping in GeTe induces the ferromagnetism while keeping the polar crystal structure (Fig. 1A) (*21*, *22*), which may enable the current-driven magnetization switching through the bulk Rashba-Edelstein effect. Although these experiments have been performed in magnetic semiconductors (*5*) and ferromagnetic metals without inversion symmetry (*23*), the ferromagnetic bulk Rashba system has an additional merit in terms of the spintronic functionality. The bulk ferroelectric polarity is characteristic of bulk Rashba systems and has a one-to-one correspondence with the spin-momentum locking manner of the Rashba effect; therefore, we can expect the electrical switching of the generated spin moments by switching of the ferroelectric polarity (*24*). In addition, ferromagnetism possibly causes the exchange-gap opening of the inner Rashba band with the originally massless Dirac dispersion (see Fig. 1B). This anticrossing-type gap formation is ubiquitous in itinerant magnets with spin-orbit interaction, where the Berry curvature governs the intrinsic anomalous Hall conductivity (σ_{AHE}) (*25*). Under this situation, σ_{AHE} is strongly enhanced as the Fermi level (E_F) becomes close to the gap region—the original position of band-crossing point. The most typical example of this is the quantum anomalous Hall effect in magnetic topological insulators (*26*, *27*). The emergence of large anomalous Hall effect and current-induced magnetization switching in the ferromagnetic Rashba system with E_F in the gapped band-crossing point are viewed as the magnetoelectric effect in semiconductor multiferroics (*28*–*30*).

(Ge,Mn)Te is a suitable platform for the effect owing to concomitance of large spin-split band and ferromagnetic order. The parent compound GeTe is a semiconductor that lacks inversion symmetry by the polar distortion with the displacement of Ge and Te ions along the [111] direction (Fig. 1A). The structural/ferroelectric phase transition temperature T_C^{FE} is approximately 700 K (*31*). The polar crystal structure leads to the finite Rashba-type band splitting. The Rashba parameter of the valence band for GeTe is α_R = 2 to 4 eV·Å (*19*, *32*), which is as large as that of the representative polar semiconductor BiTeI (*16*). Here, because of the natural tendency of Ge deficiency, GeTe tends to be a p-type degenerate semiconductor. Besides its polar semiconducting feature, GeTe can be endowed with the ferromagnetic order by Mn doping. The ferromagnetic transition temperature T_C^{FM} depends on Mn content and degree of lattice distortion (*22*). The highest T_C^{FM} reaches 150 K with Mn content around 10%. The polar structure persists up to the critical Mn content, the value of which is approximately 30 and 12% for thin film and bulk crystal, respectively (*21*, *22*).

The ferromagnetic order with the spin moments normal to the film plane modifies the Rashba-type splitting of the valence band, as schematically drawn in Fig. 1B. In the paramagnetic condition above T_C^{FM}, there is a degeneracy point where the two spin-split bands cross with each other (depicted as broken lines in Fig. 1B). Below T_C^{FM}, by contrast, breaking of time reversal symmetry opens a gap at the degeneracy point via the exchange coupling of the holes with the Mn spin moments, leading to the anticrossing of the two

[1]RIKEN Center for Emergent Matter Science (CEMS), Wako 351-0198, Japan. [2]Department of Applied Physics and Quantum-Phase Electronics Center (QPEC), University of Tokyo, Tokyo 113-8656, Japan. [3]Institute for Materials Research, Tohoku University, Sendai 980-8577, Japan. [4]PRESTO, Japan Science and Technology Agency, Chiyoda-ku, Tokyo 102-0075, Japan.
*Corresponding author. Email: ryutaro.yoshimi@riken.jp

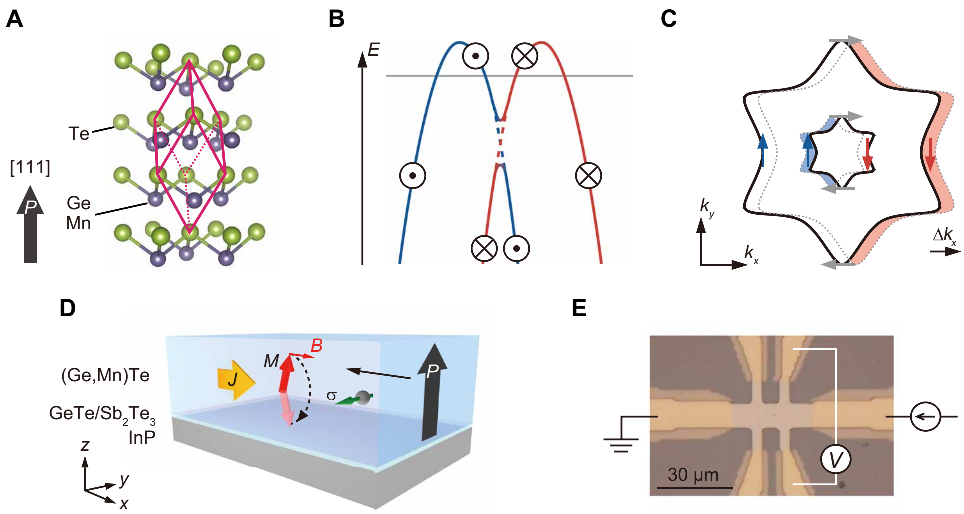

Fig. 1. Rashba-Edelstein effect in ferromagnetic Rashba semiconductor (Ge,Mn)Te. (**A**) Crystal structure of (Ge,Mn)Te with polar broken inversion symmetry along [111] denoted as *P*. A unit cell of (Ge,Mn)Te is represented as red lines. (**B**) Rashba-type spin-polarized band (valence band) by opening the magnetization gap due to broken time-reversal symmetry by ferromagnetic order. Broken lines represent the band structure above the ferromagnetic transition temperature at which the magnetization gap is closed. (**C**) Principle of Edelstein effect: The application of electric field along the *x* direction causes the shift in Fermi surfaces (represented as Δk_x), resulting in spin accumulation. The black solid and dotted lines represent the Fermi surfaces without and with the application of electric field, respectively. (**D**) Schematic illustration of magnetization switching in (Ge,Mn)Te caused by current-induced spin-orbit torque. (**E**) Top-view photograph of a Hall bar device and illustration of measurement configuration.

bands (solid lines in Fig. 1B). When E_F locates above the anticrossing gap (gray line in Fig. 1B), which is a typical case in this compound, there are two Fermi circles with different radii as shown in Fig. 1C. When the electric field is applied along the *x* direction, the respective Fermi circles shift in the opposite directions (depicted as Δk_x in Fig. 1C) owing to the opposite Fermi velocities between the inner and outer Fermi circles, resulting in the emergence of the nonequilibrium spin accumulation that can cause the current-induced magnetization switching (Fig. 1D). The total spin accumulation is the difference in contributions from the two bands. In this study, we examined the thickness and hole density dependence of the anomalous Hall conductivity and the efficiency of the Rashba-Edelstein effect in the ferromagnetic bulk Rashba semiconductor (Ge,Mn)Te thin films.

RESULTS

Transport properties and anomalous Hall effect

We have grown (Ge,Mn)Te thin films on InP (111) substrates by molecular beam epitaxy (MBE). The composition of Mn was set to 9.1 atomic % to induce the ferromagnetic order and to sustain the polar crystal structure. The Rashba parameter of this composition is evaluated as approximately 2 eV·Å by photoemission spectroscopy (*32*). The polar crystal structure of our samples was confirmed using x-ray diffraction (see fig. S1). Here, we inserted Sb_2Te_3 (1 nm) and GeTe (14 nm) as buffer layers to induce the rhombohedral lattice distortion in the Mn-doped films, which led to the higher T_C^{FM} of ~80 K than in films with the same Mn content grown directly on a substrate (*22*). Hole density *p* of the films unintentionally varies in the range of 1×10^{20} to 5×10^{20} cm^{-3} with the variation of film thickness, although the films with the thickness ranging from 22 to 192 nm were prepared at the identical growth condition. The difficulty in *p* control is probably linked to the fact that the Ge deficiency is sensitive to the growth condition such as thermal process and lattice distortion (*21*). The thickness was tuned by the growth duration by supplying identical Ge, Mn, and Te fluxes. The electrical transport properties were measured using the physical properties measurement system (PPMS; Quantum Design). The 10-µm-wide Hall bar devices (Fig. 1E) are defined using the photolithography technique (see Materials and Methods).

The Hall resistivity R_{yx} as a function of magnetic field *B* is exemplified in Fig. 2A for a 192-nm-thick sample. At T = 200 K, which is higher than T_C^{FM}, R_{yx} shows a negative slope below 0.2 T, with an ordinary positive slope at high magnetic field (black line in Fig. 2A). Such a behavior of R_{yx} typically originates from the coexistence of two types of charge carriers; electron-type (inner Fermi surface) and hole-type (outer Fermi surface) carriers contribute to R_{yx} in (Ge,Mn)Te when E_F locates above the degeneracy point in the spin-split band, as shown in Fig. 1B (the detailed temperature dependence of R_{yx} is shown in the Supplementary Materials). This E_F location is verified by a model calculation of the gapped Rashba band based on the recent results of photoemission spectroscopy (*32*) and hole density *p* (see fig. S2). When the system is ferromagnetic at T = 10 K, by contrast, R_{yx} (shown in red line) represents a clear hysteresis at a low magnetic field region, showing the anomalous Hall effect accompanied by the positive ordinary Hall response. The number of hole density *p* was evaluated from the slope at a high magnetic field region.

To elucidate the anomalous Hall effect in the ferromagnetic Rashba system, we compared the anomalous Hall conductivity σ_{AHE} in Fig. 2B for 22-, 74-, 144-, and 192-nm-thick samples that have different carrier densities; here, the anomalous Hall conductivity σ_{AHE} is defined by the subtraction of ordinary Hall component from σ_{xy} (see fig. S3). The magnetic hystereses of the four samples have similar coercive fields H_C ~ 0.15 T but have large differences in magnitude of σ_{AHE}. It is worth noting that the tiny humps are observed at around zero field; these may originate from the topological

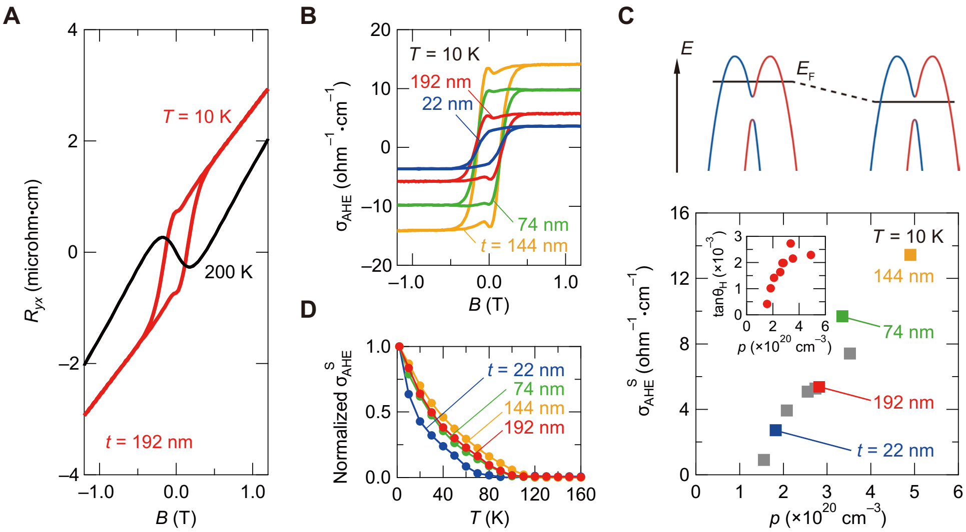

Fig. 2. Transport properties of (Ge,Mn)Te. (**A**) Magnetic field dependence of Hall resistivity R_{yx} for a 192-nm-thick (Ge,Mn)Te film at temperatures of $T = 10$ K ($<T_C^{FM}$; red) and 200 K ($>T_C^{FM}$; black); the ferromagnetic transition temperature T_C^{FM} is approximately 80 K [see (D)]. (**B**) Magnetic field dependence of anomalous Hall component in Hall conductivity σ_{AHE} at $T = 10$ K for (Ge,Mn)Te thin films with thicknesses of 22, 74, 144, and 192 nm. (**C**) Top: Ferromagnetic Rashba band structures with E_F above (left) and within (right) the exchange gap. Bottom: Hole concentration (p) dependence of spontaneous anomalous Hall conductivity σ_{AHE}^S at $T = 10$ K for all the measured samples with different thicknesses and p values. The inset shows the p dependence of the Hall angle $\tan\theta_H$. (**D**) Temperature dependence of σ_{AHE}^S normalized by the value at the lowest temperature $T = 2$ K for the films with various thicknesses.

Hall effect that is characteristic of noncoplanar spin configuration with scaler spin chirality, like magnetic skyrmion, in the magnetic systems without inversion symmetry (*33*, *34*). The hole density p dependence of the spontaneous component σ_{AHE}^S (defined as σ_{AHE} at $B = 0$) is summarized in Fig. 2C (see fig. S3 for other samples); σ_{AHE}^S shows a large variation ranging from 0.9 to 13 ohm^{-1} cm^{-1}. The clear correlation between σ_{AHE}^S and p is in accord with the Berry phase scenario that the anomalous Hall conductivity is enhanced in magnitude as E_F becomes close to the magnetization-induced gap (schematically depicted in the top right panel of Fig. 2C). Similar to σ_{AHE}^S, the anomalous Hall angle $\tan\theta_H$, defined as $\sigma_{AHE}^S/\sigma_{xx}(0\ T)$, shows the monotonic increasing behavior with p (shown in the inset of Fig. 2C). The value $\tan\theta_H = 2 \times 10^{-3}$ to 3×10^{-3} is a typical or slightly smaller value compared with other magnets such as elemental transition ferromagnets (*25*), permalloy (*35*), CoFeB (*36*), diluted magnetic semiconductor (*37*), and noncollinear antiferromagnet (*38*). The temperature dependence of σ_{AHE}^S for various samples (Fig. 2D) indicates that $T_C^{FM} \sim 80$ K is almost independent of samples. The minimal thickness dependence of H_C and T_C^{FM} in the film ensures homogeneous quality of thin films along the thickness direction as well as little effect from the surface or interface. The notable E_F-dependent variation in anomalous Hall conductivity verifies the dominant contribution of Berry phase generated at the magnetization-induced gap (band anticrossing point) in the ferromagnetic Rashba system.

Current-driven magnetization switching

One of the emergent functions of such a multiferroic semiconductor with ferromagnetic Rashba bands is the exertion of spin-orbit torque by the spin-polarized current, which may realize the current-driven magnetization switching (*1*, *9*, *10*, *12*–*15*). The current-driven magnetization switching experiment was performed at $T = 10$ K ($<T_C^{FM}$). The spin accumulation was generated by the injection of pulse currents under the application of small in-plane magnetic field of 0.02 T, which was necessary to determine the final state of the magnetization (see Materials and Methods). To minimize the heating effect of the sample, we set the maximum current density to 6×10^6 A cm^{-2} in this experiment. After each pulse injection, the Hall resistivity R_{yx}^{pulse} was measured by the small excitation current (see Materials and Methods) to remove the current-nonlinear contribution of magnon scattering that was pointed out for the case of a magnetic topological insulator (*10*). Figure 3A shows the change in Hall resistivity ΔR_{yx}^{pulse} for four different thickness samples as a function of the injected current density j (see fig. S5 for other samples). All the samples show similar behaviors. Upon the positive (negative) current pulse under positive 0.02 T (red lines), R_{yx}^{pulse} starts to change at around $j \sim +2 \times 10^6$ (-2×10^6) A cm^{-2} by opening a hysteresis in the reversed scan. The hysteresis direction is reversed when the in-plane magnetic field is reversed (blue lines), verifying that the magnetization is switched by the current-driven spin-orbit torque.

In this measurement range, the maximum value of ΔR_{yx}^{pulse} is ~0.05 microhm·cm, which is approximately 10% of the full magnetization reversal (the Hall resistivity for the full magnetization is shown in the Supplementary Materials). One possible reason for the limited magnetization reversal is the insufficient current density used in this experiment to avoid the heating-induced damage in the thin film. Nevertheless, the sample temperature may increase at high j region, and an intermediate magnetic state may appear with randomly distributed domains, which leads to the saturation of ΔR_{yx}^{pulse} (Fig. 3A) and makes the full reversal difficult. However, the magnitude of j used in this experiment is an order of magnitude smaller than that used in other magnetic materials and 2D Rashba interfaces/surfaces. In addition to small j, because of the warping effect of the band dispersion in this material (Fig. 1C), the spin polarization of the band tends to cant to the out-of-plane direction (*32*), which may decrease the in-plane spin polarization and efficiency

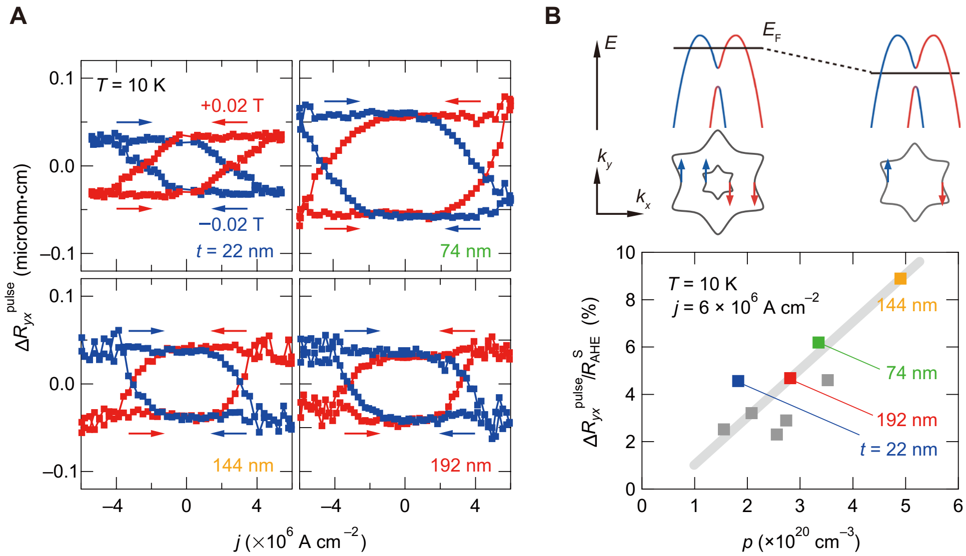

Fig. 3. Experimental observation of current-driven magnetization switching. (**A**) Variation in Hall resistivity ΔR_{yx}^{pulse} by current pulse injection for (Ge,Mn)Te thin films with thicknesses of 22, 74, 144, and 192 nm. Red and blue traces correspond to the cases of the in-plane bias magnetic field of +0.02 and −0.02 T, respectively, which are applied along the current direction (depicted in Fig. 1D). (**B**) Top: Schematic view of the E_F shift in ferromagnetic Rashba bands and change in Fermi surface at E_F. Bottom: Hole concentration (p) dependence of switching ratio of Hall resistivity defined as $\Delta R_{yx}^{pulse}/R_{AHE}^{S}$.

of spin-charge conversion (*18*). As for the warping effect of the Fermi surface, we have performed the current directional dependence but we observed no discernible difference (see fig. S6). The observation in the (Ge,Mn)Te film as thick as 200 nm exemplifies the bulk-origin Rashba-Edelstein effect, not from surface- or interface-originated one.

DISCUSSION

The Edelstein effect also depends on E_F position in the ferromagnetic Rashba band, as shown in the top panel of Fig. 3B. The bottom panel of Fig. 3B shows the hole density dependence of the switching ratio, which is defined as the ratio between ΔR_{yx}^{pulse} at $j = 6 \times 10^6$ A cm^{-2} and the spontaneous anomalous Hall resistivity R_{AHE}^{S} (R_{yx} at $B = 0$ T). As an overall behavior, the switching ratio increases with increasing hole density. This also supports the change in E_F position as discussed in Fig. 2C. As the hole density increases, E_F becomes closer to the magnetization-induced gap in the inner Rashba band. This gives the shrinking of the inner Fermi surface that suppresses the cancellation of the spin accumulation from the inner and outer bands, as schematically shown in Fig. 3B. The E_F-sensitive magnetization switching exemplifies the unique band structure of the ferromagnetic Rashba system to cause the Rashba-Edelstein effect.

In conclusion, we have successfully observed the current-driven magnetization switching in bulk Rashba ferromagnet (Ge,Mn)Te thin films. The injection of pulse current switches the bulk magnetization even in a 192-nm-thick film, which evidences the Rashba-Edelstein effect of bulk origin. Furthermore, the strong E_F dependence of the anomalous Hall conductivity and the efficiency of magnetization switching are observed to reflect the bulk band structure of the ferromagnetic Rashba system. These results demonstrate the correlation between electric polarization and magnetization in the ferromagnetic Rashba system as a semiconductor multiferroic.

MATERIALS AND METHODS

Thin-film growth and device fabrication

(Ge,Mn)Te films were fabricated with buffer layers GeTe (14 nm)/Sb_2Te_3 (1 nm) on semi-insulating InP (111) substrates at 200°C by MBE. The epi-ready substrate was annealed at 340°C in vacuum before the epitaxy. The equivalent pressure of beam flux for Ge, Mn, and Te is 4.5×10^{-6} Pa, 5.0×10^{-7} Pa, and 5.0×10^{-5} Pa, respectively. The Mn composition of 9.1 atomic % was evaluated from the inductively coupled plasma mass spectroscopy measurement. The growth rate of (Ge,Mn)Te was approximately 2.5 nm/min. After the thin-film growth, Hall bar devices with 10 μm in both width and length were defined using ultraviolet photolithography and Ar ion milling. The electrodes Au (25 nm)/Ti (5 nm) were formed by electron beam deposition.

Transport measurement and magnetization switching

Transport measurements were conducted using the DC transport option of PPMS (Quantum Design). The procedure of magnetization switching was as follows. (i) The in-plane magnetic field of 3 T was applied for the initialization of the magnetization. (ii) Under a small in-plane magnetic field, a single pulse current with a duration of 1 ms was injected. (iii) The anomalous Hall resistance was measured with low current (1 mA). (iv) Steps (ii) and (iii) were repeated by varying the pulse height of (ii). We used the Keithley model 6221 as the current source and the Keithley model 2182A as the voltmeter. We made the correction of current density by considering the parallel conduction in buffer layers whose resistivity is 2.5 milliohm·cm at 10 K. Because the resistivity of semi-insulating InP substrate was 10 megohm·cm even at room temperature and became completely insulating at low temperature, we did not need to take into account any parallel conduction in the substrate. During the magnetization switching measurement, the sample temperature was kept at 10 K using the cooling system of PPMS.

SUPPLEMENTARY MATERIALS

Supplementary material for this article is available at http://advances.sciencemag.org/cgi/content/full/4/12/eaat9989/DC1

Section S1. Determination of lattice constants for (Ge,Mn)Te thin films by x-ray diffraction
Section S2. Qualitative evaluation of E_F in (Ge,Mn)Te
Section S3. Electronic transport properties of the (Ge,Mn)Te samples
Section S4. Temperature dependence of Hall resistivity
Section S5. Current-induced magnetization reversal for all samples
Section S6. Current-directional dependence of magnetization switching
Section S7. In-plane bias magnetic field dependence of magnetization switching
Section S8. Repeated injection of pulses lower than saturation current density
Section S9. The estimation of spin Hall efficiency
Section S10. Correction of current flow to buffer layers
Section S11. Magnetization measurement
Fig. S1. Reciprocal space analysis for the in- and out-of-plane lattice constants of (Ge,Mn)Te thin film.
Fig. S2. Calculated band structure of (Ge,Mn)Te for $x = 0.08$.
Fig. S3. Transport properties for all samples.
Fig. S4. Temperature dependence of Hall resistivity.
Fig. S5. Current-induced magnetization for all samples.
Fig. S6. Current-directional dependence of magnetization switching.
Fig. S7. In-plane bias magnetic field dependence of magnetization switching.
Fig. S8. Repeated injection of pulses lower than saturation current density.
Fig. S9. Second-harmonic Hall resistivity.
Fig. S10. Temperature dependence of resistivity of the GeTe/Sb_2Te_3 thin film.
Fig. S11. Magnetization measurement for 74- and 192-nm-thick samples.
Table S1. Physical parameters for the effective band model of (Ge,Mn)Te.
Table S2. Current ratio for all samples.
References (*39–41*)

REFERENCES AND NOTES

1. A. Manchon, H. C. Koo, J. Nitta, S. M. Frolov, R. A. Duine, New perspectives for Rashba spin-orbit coupling. *Nat. Mater.* **14**, 871–882 (2015).
2. E. I. Rashba, Properties of semiconductors with an extremum loop. I. Cyclotron and combinational resonance in a magnetic field perpendicular to the plane of the loop. *Phys. Solid State* **2**, 1109–1122 (1960).
3. G. Dresselhaus, Spin-orbit coupling effects in zinc blende structures. *Phys. Rev.* **100**, 580–586 (1955).
4. V. M. Edelstein, Spin polarization of conduction electrons induced by electric current in two-dimensional asymmetric electron systems. *Solid State Commun.* **73**, 233–235 (1990).
5. A. Chernyshov, M. Overby, X. Liu, J. K. Furdyna, Y. Lyanda-Geller, L. P. Rokhinson, Evidence for reversible control of magnetization in a ferromagnetic material by means of spin–orbit magnetic field. *Nat. Phys.* **5**, 656–659 (2009).
6. D. Fang, H. Kurebayashi, J. Wunderlich, K. Výborný, L. P. Zârbo, R. P. Campion, A. Casiraghi, B. L. Gallagher, T. Jungwirth, A. J. Ferguson, Spin-orbit-driven ferromagnetic resonance. *Nat. Nanotechnol.* **6**, 413–417 (2011).
7. J.-C. Rojas-Sánchez, L. Vila, G. Desfonds, S. Gambarelli, J. P. Attané, J. M. De Teresa, C. Magén, A. Fert, Spin-to-charge conversion using Rashba coupling at the interface between non-magnetic materials. *Nat. Commun.* **4**, 2944 (2013).
8. E. Lesne, Y. Fu, S. Oyarzun, J. C. Rojas-Sánchez, D. C. Vaz, H. Naganuma, G. Sicoli, J.-P. Attané, M. Jamet, E. Jacquet, J.-M. George, A. Barthélémy, H. Jaffrès, A. Fert, M. Bibes, L. Vila, Highly efficient and tunable spin-to-charge conversion through Rashba coupling at oxide interfaces. *Nat. Mater.* **15**, 1261–1266 (2016).
9. Y. Fan, P. Upadhyaya, X. Kou, M. Lang, S. Takei, Z. Wang, J. Tang, L. He, L.-T. Chang, M. Montazeri, G. Yu, W. Jiang, T. Nie, R. N. Schwartz, Y. Tserkovnyak, K. L. Wang, Magnetization switching through giant spin-orbit torque in a magnetically doped topological insulator heterostructure. *Nat. Mater.* **13**, 699–704 (2014).
10. K. Yasuda, A. Tsukazaki, R. Yoshimi, K. Kondou, K. S. Takahashi, Y. Otani, M. Kawasaki, Y. Tokura, Current-nonlinear Hall effect and spin-orbit torque magnetization switching in a magnetic topological insulator. *Phys. Rev. Lett.* **119**, 137204 (2017).
11. K. Kondou, R. Yoshimi, A. Tsukazaki, Y. Fukuma, J. Matsuno, K. S. Takahashi, M. Kawasaki, Y. Tokura, Y. Otani, Fermi-level-dependent charge-to-spin current conversion by Dirac surface states of topological insulators. *Nat. Phys.* **12**, 1027–1031 (2016).
12. J. Han, A. Richardella, S. A. Siddiqui, J. Finley, N. Samarth, L. Liu, Room-temperature spin-orbit torque switching induced by a topological insulator. *Phys. Rev. Lett.* **119**, 077702 (2017).
13. Y. Wang, D. Zhu, Y. Wu, Y. Yang, J. Yu, R. Ramaswamy, R. Mishra, S. Shi, M. Elyasi, K.-L. Teo, Y. Wu, H. Yang, Room temperature magnetization switching in topological insulator-ferromagnet heterostructures by spin-orbit torques. *Nat. Commun.* **8**, 1364 (2017).
14. M. Dc, R. Grassi, J.-Y. Chen, M. Jamali, D. Reifsnyder Hickey, D. Zhang, Z. Zhao, H. Li, P. Quarterman, Y. Lv, M. Li, A. Manchon, K. Andre Mkhoyan, T. Low, J.-P. Wang, Room-temperature high spin-orbit torque due to quantum confinement in sputtered $Bi_xSe_{(1-x)}$ films. *Nat. Mater.* **17**, 800–807 (2018).
15. N. H. D. Khang, Y. Ueda, P. N. Hai, A conductive topological insulator with large spin Hall effect for ultralow power spin-orbit torque switching. *Nat. Mater.* **17**, 808–813 (2018).
16. K. Ishizaka, M. S. Bahramy, H. Murakawa, M. Sakano, T. Shimojima, T. Sonobe, K. Koizumi, S. Shin, H. Miyahara, A. Kimura, K. Miyamoto, T. Okuda, H. Namatame, M. Taniguchi, R. Arita, N. Nagaosa, K. Kobayashi, Y. Murakami, R. Kumai, Y. Kaneko, Y. Onose, Y. Tokura, Giant Rashba-type spin splitting in bulk BiTeI. *Nat. Mater.* **10**, 521–526 (2011).
17. M. Sakano, M. S. Bahramy, A. Katayama, T. Shimojima, H. Murakawa, Y. Kaneko, W. Malaeb, S. Shin, K. Ono, H. Kumigashira, R. Arita, N. Nagaosa, H. Y. Hwang, Y. Tokura, K. Ishizaka, Strongly spin-orbit coupled two-dimensional electron gas emerging near the surface of polar semiconductors. *Phys. Rev. Lett.* **110**, 107204 (2013).
18. C. Rinaldi, J. C. Rojas-Sánchez, R. N. Wang, Y. Fu, S. Oyarzun, L. Vila, S. Bertoli, M. Asa, L. Baldrati, M. Cantoni, J.-M. George, R. Calarco, A. Fert, R. Bertacco, Evidence for spin to charge conversion in GeTe(111). *APL Mater.* **4**, 032501 (2016).
19. M. Liebmann, C. Rinaldi, D. Di Sante, J. Kellner, C. Pauly, R. N. Wang, J. E. Boschker, A. Giussani, S. Bertoli, M. Cantoni, L. Baldrati, M. Asa, I. Vobornik, G. Panaccione, D. Marchenko, J. Sánchez-Barriga, O. Rader, R. Calarco, S. Picozzi, R. Bertacco, M. Morgenstern, Giant Rashba-type spin splitting in ferroelectric GeTe(111). *Adv. Mater.* **28**, 560–565 (2016).
20. D. Di Sante, P. Barone, R. Bertacco, S. Picozzi, Electric control of the giant Rashba effect in bulk GeTe. *Adv. Mater.* **25**, 509–513 (2013).
21. M. Kriener, T. Nakajima, Y. Kaneko, A. Kikkawa, X. Z. Yu, N. Endo, K. Kato, M. Takata, T. Arima, Y. Tokura, Y. Taguchi, Heat-treatment-induced switching of magnetic states in the doped polar semiconductor $Ge_{1-x}Mn_xTe$. *Sci. Rep.* **6**, 25748 (2016).
22. H. Przybylinska, G. Springholz, R. T. Lechner, M. Hassan, M. Wegscheider, W. Jantsch, G. Bauer, Magnetic-field-induced ferroelectric polarization reversal in the multiferroic $Ge_{1-x}Mn_xTe$ semiconductor. *Phys. Rev. Lett.* **112**, 047202 (2014).
23. C. Ciccarelli, L. Anderson, V. Tshitoyan, A. J. Ferguson, F. Gerhard, C. Gould, L. W. Molenkamp, J. Gayles, J. Železný, L. Šmejkal, Z. Yuan, J. Sinova, F. Freimuth, T. Jungwirth, Room-temperature spin–orbit torque in NiMnSb. *Nat. Phys.* **12**, 855–860 (2016).
24. C. Rinaldi, S. Varotto, M. Asa, J. Sławińska, J. Fujii, G. Vinai, S. Cecchi, D. Di Sante, R. Calarco, I. Vobornik, G. Panaccione, S. Picozzi, R. Bertacco, Ferroelectric control of the spin texture in GeTe. *Nano Lett.* **18**, 2751–2758 (2018).
25. N. Nagaosa, J. Sinova, S. Onoda, A. H. MacDonald, N. P. Ong, Anomalous Hall effect. *Rev. Mod. Phys.* **82**, 1539–1592 (2010).
26. C. Z. Chang, J. Zhang, X. Feng, J. Shen, Z. Zhang, M. Guo, K. Li, Y. Ou, P. Wei, L.-L. Wang, Z.-Q. Ji, Y. Feng, S. Ji, X. Chen, J. Jia, X. Dai, Z. Fang, S.-C. Zhang, K. He, Y. Wang, L. Lu, X.-C. Ma, Q.-K. Xue, Experimental observation of the quantum anomalous Hall effect in a magnetic topological insulator. *Science* **340**, 167–170 (2013).
27. J. G. Checkelsky, R. Yoshimi, A. Tsukazaki, K. S. Takahashi, Y. Kozuka, J. Falson, M. Kawasaki, Y. Tokura, Trajectory of the anomalous Hall effect towards the quantized state in a ferromagnetic topological insulator. *Nat. Phys.* **10**, 731–736 (2014).
28. X.-L. Qi, T. L. Hughes, S.-C. Zhang, Topological field theory of time-reversal invariant insulators. *Phys. Rev. B* **78**, 195424 (2008).
29. F. Matsukura, Y. Tokura, H. Ohno, Control of magnetism by electric fields. *Nat. Nanotechnol.* **10**, 209–220 (2015).
30. W. Eerenstein, N. D. Mathur, J. F. Scott, Multiferroic and magnetoelectric materials. *Nature* **442**, 759–765 (2006).
31. T. Chattopadhyay, J. X. Boucherle, H. G. von Schnering, Neutron diffraction study on the structural phase transition in GeTe. *J. Phys. C Solid State Phys.* **20**, 1431–1440 (1987).
32. J. Krempasky, S. Muff, F. Bisti, M. Fanciulli, H. Volfová, A. P. Weber, N. Pilet, P. Warnicke, H. Ebert, J. Braun, F. Bertran, V. V. Volobuev, J. Minár, G. Springholz, J. H. Dil, V. N. Strocov, Entanglement and manipulation of the magnetic and spin–orbit order in multiferroic Rashba semiconductors. *Nat. Commun.* **7**, 13071 (2016).
33. J. Matsuno, N. Ogawa, K. Yasuda, F. Kagawa, W. Koshibae, N. Nagaosa, Y. Tokura, M. Kawasaki, Interface-driven topological Hall effect in $SrRuO_3$-$SrIrO_3$ bilayer. *Sci. Adv.* **2**, e1600304 (2016).
34. K. Yasuda, R. Wakatsuki, T. Morimoto, R. Yoshimi, A. Tsukazaki, K. S. Takahashi, M. Ezawa, M. Kawasaki, N. Nagaosa, Y. Tokura, Geometric Hall effects in topological insulator heterostructures. *Nat. Phys.* **12**, 555–559 (2016).
35. Y. Q. Zhang, N. Y. Sun, R. Shan, J. W. Zhang, S. M. Zhou, Z. Shi, G. Y. Guo, Anomalous Hall effect in epitaxial permalloy thin films. *J. Appl. Phys.* **114**, 163714 (2013).
36. Y. Zhang, W. Mi, X. Wang, Z. Guo, Scaling of anomalous Hall effect in amorphous CoFeB films with accompanying quantum correction. *Solid State Commun.* **215–216**, 5–11 (2015).
37. D. Chiba, A. Werpachowska, M. Endo, Y. Nishitani, F. Matsukura, T. Dietl, H. Ohno, Anomalous Hall effect in field-effect structures of (Ga,Mn)As. *Phys. Rev. Lett.* **104**, 106601 (2010).
38. S. Nakatsuji, N. Kiyohara, T. Higo, Large anomalous Hall effect in a non-collinear antiferromagnet at room temperature. *Nature* **527**, 212–215 (2015).

39. J.-C. Rojas-Sánchez, P. Laczkowski, J. Sampaio, S. Collin, K. Bouzehouane, N. Reyren, H. Jaffrès, A. Mougin, J.-M. George, Perpendicular magnetization reversal in Pt/[Co/Ni]$_3$/Al multilayers via the spin Hall effect of Pt. *Appl. Phys. Lett.* **108**, 082406 (2016).
40. J. Kim, J. Sinha, M. Hayashi, M. Yamanouchi, S. Fukami, T. Suzuki, S. Mitani, H. Ohno, Layer thickness dependence of the current-induced effective field vector in Ta|CoFeB|MgO. *Nat. Mater.* **12**, 240–245 (2013).
41. H. Ohno, A. Shen, F. Matsuka, A. Oiwa, A. Endo, S. Katsumoto, Y. Iye, (Ga,Mn)As: A new diluted magnetic semiconductor based on GaAs. *Appl. Phys. Lett.* **69**, 363–365 (1996).

Acknowledgments: We thank K. Kondou and M. Kawamura for fruitful discussion. **Funding:** This research was supported by JSPS/MEXT Grant-in-Aid for Scientific Research(s) (grant nos. 24224009, 24226002, JP17H04846, JP18H04229, and JP15H05853) and CREST, JST (grant no. JPMJCR16F1). **Author contributions:** Y.T. conceived the project. R.Y. performed the thin-film growth, device fabrication, DC transport measurements, and data analysis. R.Y. and K.Y. performed the magnetization switching measurement. R.Y., A.T., and Y.T. wrote the manuscript with contributions from all authors. **Competing interests:** The authors declare that they have no competing interests. **Data and materials availability:** All data needed to evaluate the conclusions in the paper are present in the paper and/or the Supplementary Materials. Additional data related to this paper may be requested from the authors.

Submitted 26 April 2018
Accepted 6 November 2018
Published 7 December 2018
10.1126/sciadv.aat9989

Citation: R. Yoshimi, K. Yasuda, A. Tsukazaki, K. S. Takahashi, M. Kawasaki, Y. Tokura, Current-driven magnetization switching in ferromagnetic bulk Rashba semiconductor (Ge,Mn)Te. *Sci. Adv.* **4**, eaat9989 (2018).

Science Advances

Current-driven magnetization switching in ferromagnetic bulk Rashba semiconductor (Ge,Mn)Te

R. Yoshimi, K. Yasuda, A. Tsukazaki, K. S. Takahashi, M. Kawasaki and Y. Tokura

Sci Adv **4** (12), eaat9989.
DOI: 10.1126/sciadv.aat9989